Edge-carboxylated graphene nanosheets via ball milling

In-Yup Jeon[a], Yeon-Ran Shin[a], Gyung-Joo Sohn[a], Hyun-Jung Choi[a], Seo-Yoon Bae[a], Javeed Mahmood[a], Sun-Min Jung[a], Jeong-Min Seo[a], Min-Jung Kim[a], Dong Wook Chang[a,b], Liming Dai[a,c,1], and Jong-Beom Baek[a,1]

[a]Interdisciplinary School of Green Energy/Low-dimensional Carbon Materials Center, Ulsan National Institute of Science and Technology (UNIST), 100 Banyeon, Ulsan 689-798, South Korea; [b]Department of Chemical Systematic Engineering, Catholic University of Daegu, 13-13 Hayang, Gyungbuk, 712-702, South Korea; and [c]Department of Macromolecular Science and Engineering, Case Western Reserve University, 10900 Euclid Avenue, Cleveland, Ohio 44106

Edited by Hui-Ming Cheng, Institute of Metal Research, Chinese Academy of Sciences, Shenyang, China, and accepted by the Editorial Board February 8, 2012 (received for review October 13, 2011)

Low-cost, high-yield production of graphene nanosheets (GNs) is essential for practical applications. We have achieved high yield of edge-selectively carboxylated graphite (ECG) by a simple ball milling of pristine graphite in the presence of dry ice. The resultant ECG is highly dispersable in various solvents to self-exfoliate into single- and few-layer (≤5 layers) GNs. These stable ECG (or GN) dispersions have been used for solution processing, coupled with thermal decarboxylation, to produce large-area GN films for many potential applications ranging from electronic materials to chemical catalysts. The electrical conductivity of a thermally decarboxylated ECG film was found to be as high as 1214 S/cm, which is superior to its GO counterparts. Ball milling can thus provide simple, but efficient and versatile, and eco-friendly (CO_2-capturing) approaches to low-cost mass production of high-quality GNs for applications where GOs have been exploited and beyond.

carbon dioxide | eco-friendly | edge-functionalization | graphite

As a building block for carbon nanomaterials of all other dimensionalities, such as 0D buckyball, 1D nanotubes, and 3D graphite, graphene nanosheets (GNs) with carbon atoms densely packed in a 2D honeycomb crystal lattice have recently attracted tremendous interest for various potential applications (1). Several techniques, including the peel-off by Scotch tape (2), epitaxial growth on SiC (3), chemical vapor deposition (CVD) (4, 5), and solution exfoliation of graphite oxide (GO) (6), have been reported for producing GNs. Although the Scotch tape method led to the Nobel-Prize-winning discovery of high quality GNs (2), it is unsuitable for large-area preparation of GN films due to technique difficulties. On the other hand, large-area thin GN films up to 30 in. have been prepared by CVD (7). However, the CVD process involves extremely careful fabrication processes, which appears to be too tedious and too expensive for mass production. The widely reported solution exfoliation of graphite into GO, followed by solution reduction (8–10), allows the mass production of GNs via an all-solution process. Due to strong interactions between the hexagonally sp^2-bonded carbon layers in graphite, however, the solution exfoliation requires the involvement of hazardous strong oxidizing reagents (e.g., HNO_3, $KMnO_4$, and/or H_2SO_4) and a tedious multistep process (8, 9, 11, 12). Such a corrosive chemical oxidation often causes severe damage to the carbon basal plane to introduce a large number of chemical and topological defects (13). As a result, postexfoliation reduction of GO into reduced graphene oxide (rGO) is essential in order to restore the graphitic basal plane for the resultant GNs (6,14–19). To make the matter worse, the reduction reaction also involves hazardous reducing reagents (e.g., hydrazine, $NaBH_4$) with a limited reduction conversion (approximately 70%) (20). The reduced GO (rGO) still contains considerable oxygenated groups and structural defects, and thus additional high-temperature thermal annealing step is required (20).

To overcome the above-mentioned limitations on the widely studied GO approach, we report here a method for a simple, but effective and eco-friendly, edge-selective functionalization of graphite without the basal plane oxidation by ball milling in the presence of dry ice (solid phase of carbon dioxide). High yield of edge-carboxylated graphite (ECG) was produced and the resultant ECG is highly dispersible in various polar solvents to self-exfoliate into GNs useful for solution processing. Unlike GO, the edge-selective functionalization of the pristine graphite could preserve the high crystalline graphitic structure on its basal plane. The edge-attached functional groups tend to repel each other to effectively open up the edges of the ECG, leading to self-exfoliation in solvent for the formation of high-quality GN films. Indeed, large-area GN films with an electrical conductivity as high as 1,214 S/cm, superior to their GO counterparts, have been prepared simply by solution casting the ECG dispersions on a substrate, followed by thermal decarboxylation. In addition, the use of dry ice (or CO_2 gas) as a reagent for carboxylation in the ball milling could also facilitate the CO_2 capture and storage to reduce their detrimental effects on our planet (21). Therefore, the newly developed ball milling approach, involving neither hazardous chemicals nor tedious procedures, outperforms current processes for mass production of high-quality GNs at an unprecedented low cost.

Results and Discussion

In a typical experiment, ball milling was carried out in a planetary ball-mill machine (Pulverisette 6, Fritsch; Fig. S1*A*) in the presence of graphite (5.0 g, Fig. 1*A*), dry ice (100 g, Fig. 1*B*) and stainless steel balls (Fig. S1*B*). Detailed experimental conditions for the ball milling can be found in the *Materials and Methods* section and *Supporting Information*. Upon opening the stainless steel capsule lid (Fig. S1*C*) in air at the end of ball-milling process, violent sparkling occurred (Figs. S1*D* and *E* and Movies S1, S2, and S3), presumably due to hydration of the ball-milling-induced, highly energetic carboxylates (-COO^-) into carboxylic acids (-COOH) by air moisture (H_2O) and residual activated carbon species (radicals, anions, and cations) into hydroxyl (-OH) and hydroperoxy (-OOH) by air oxygen (O_2) and moisture (H_2O). The recovered product was further Soxhlet extracted with 1 M aqueous HCl solution to completely acidify carboxylates and to remove metallic impurities, if any. The starting graphite (Fig. 1*A*) gained weight to be 6.28 g of the ECG (Fig. 1*C*), indicating an efficient uptake of CO_2 (1.28 g). A high-yield carboxylation was thus occurred, as schematically shown in Fig. 1*D*. The

Author contributions: J.-B.B. designed research; I.-Y.J., Y.-R.S., G.-J.S., H.-J.C., S.-Y.B., J.M., S.-M.J., J.-M.S., M.-J.K., and D.W.C. performed research; I.-Y.J., L.D., and J.-B.B. analyzed data; and L.D. and J.-B.B. wrote the paper.

The authors declare no conflict of interest.

This article is a PNAS Direct Submission. H.C. is a guest editor invited by the Editorial Board.

[1]To whom correspondence may be addressed. E-mail: jbbaek@unist.ac.kr or liming.dai@case.edu.

This article contains supporting information online at www.pnas.org/lookup/suppl/doi:10.1073/pnas.1116897109/-/DCSupplemental.

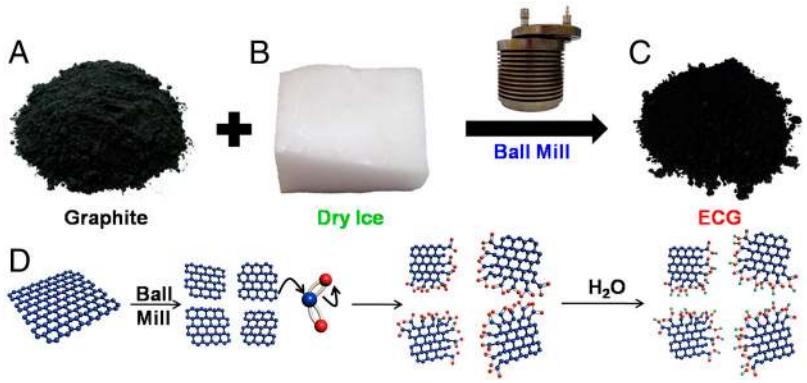

Fig. 1. (*A*) Pristine graphite; (*B*) dry ice (solid phase CO_2); (*C*) edge-carboxylated graphite (ECG) prepared by ball milling for 48 h; (*D*) a schematic representation of physical cracking and edge-carboxylation of graphite by ball milling in the presence of dry ice, and protonation through subsequent exposure to air moisture. Detailed proposed mechanism is presented in Fig. S2.

detailed mechanism of carboxylation via mechano-chemical process by ball milling is proposed in Fig. S2 and confirmed by various spectroscopic measurements (*vide infra*). Elemental (EA, Table S1) and thermogravimetric analyses (TGA, Fig. S3) revealed that the oxygen content of ECG increased with an increase in the ball-milling time before leveling off at 48 h. The increase in the ball-milling time also caused a continuous decrease in the sample grain size until 48 h to reach a steady state, as seen from the scanning electron microscope (SEM, FEI Nanonova 230) images in Fig. S4. For subsequent investigation, therefore, ECG samples prepared by the ball milling for 48 h were used unless otherwise stated. As reference, GO was also prepared by the modified Hummers' process (see, Experimental Section in *Supporting Information*) (12). Figs. S5*A* and *B* show typical SEM and transmission electron microscope [HR-TEM, JEOL JEM-2100F (Cs)] images, respectively, for the GO sample thus prepared. To empathize advantages of the ECG approach, the direct comparison between GO and ECG approaches is presented in Fig. S6.

Fig. 2*A* gives a typical SEM image of the pristine graphite flake, showing micro-scale (100 mesh, <150 μm) irregular particle grains with smooth surfaces. As proposed in Fig. 1*D*, more homogenous but much smaller ECG grains (100 ~ 500 nm) formed after ball milling for 48 h (Fig. 2*B*). The corresponding TEM images given in Figs. 2*C* and Fig. S7 clearly show the presence of GNs (Noted that the ECG have self-exfoliated into nanosheets in the dispersion used for TEM sample preparation—*Supporting Information*) with wrinkles characteristic of flexible GNs.

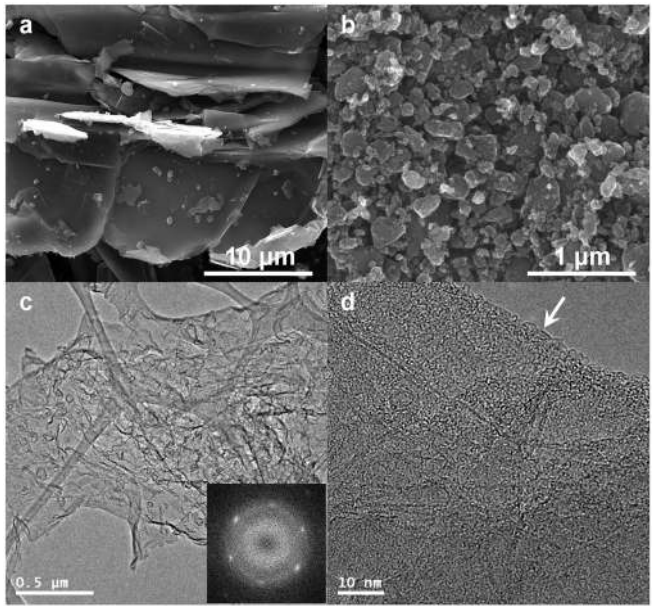

Fig. 2. SEM images: (*A*) the pristine graphite and (*B*) edge-carboxylated graphite (ECG). TEM images: (*C*) ECG at a low magnification. *Inset* shows a selected area electron diffraction (SAED) pattern, showing high crystallinity; (*D*) Edge-on view of (*C*) at a higher magnification.

Selected area electron diffraction pattern (SAED) (Fig. 2*C*, *Inset*) shows a typical sixfold symmetry peaks with the {2110} spots appeared to be more intense relative to the {1100} spots, reflecting a few layers (<5 layers, *vide infra*) of GNs with high crystallinity (22). Due to the strong van der Waals interactions associated with the defect-free basal planes and hydrogen bonding of the edge-carboxylic acids, therefore, GNs in the dip-coated ECG dispersion (0.02 mg/mL in NMP) on a TEM grid have a strong tendency to "restack" into overlapped aggregates. Under a higher magnification, the self-assembled ECG thin film showed some edge distortion, as indicated by the arrow in Fig. 2*D*. As observed on TEM (Fig. S7) and atomic force microscope (AFM) (Fig. S8), most of the GN films are typically less than five graphitic layers and single layer population is approximately 25% (Fig. S8*A*). The above results clearly indicate that the pristine graphite flake could have been directly exfoliated into single and few-layer GNs simply by ball milling in the presence of dry ice, followed by dispersion in polar solvents (*vide infra*).

From EA data (i.e., an oxygen content of 26.46% and C/O = 3.63, Table S1) for ECG ball milled 48h, we can estimated that an average one carboxylic acid group has been introduced onto every 7.26 carbons along the distorted ECG edge if there is negligible carboxylation on the basal plane. This is in good consistence with the TGA results (see, Table S2 and Fig. S3). To gain further insights on chemical changes caused by the ball milling, we performed Fourier transform infrared (FTIR) spectroscopic measurements. FTIR spectrum of the pristine graphite (Fig. 3*A*) shows only a weak band at 1,632 cm^{-1} characteristic of the vibration mode of adsorbed water molecules (23) in addition to the strong peak at 3,400 cm^{-1} attributable to crystal water associated with KBr used for the preparation of IR specimen. However, the presence of carboxylic acid groups in ECG and GO is clearly evident by a strong C = O stretching peak at 1,718 cm^{-1} seen in Fig. 3*A*. As expected, the FTIR spectrum of ECG shows a unique sharp peak for C–O stretching at 1,250 cm^{-1} exclusively from O = C-OH (see, Fig. S6*B*) whereas the corresponding broad C–O stretching band for GO indicates the coexistence of C–OH (hydroxyl), C–O–C (epoxy) and O = C-OH (carboxyl) (see, Fig. S6*A*). Hydroxyl and epoxy groups have been known to distribute over the carbon basal plane while carboxyl groups are mainly located at the edge in GO (24, 25). This, once again, implies the edge-carboxylation for ECG. Both ECG and GO display

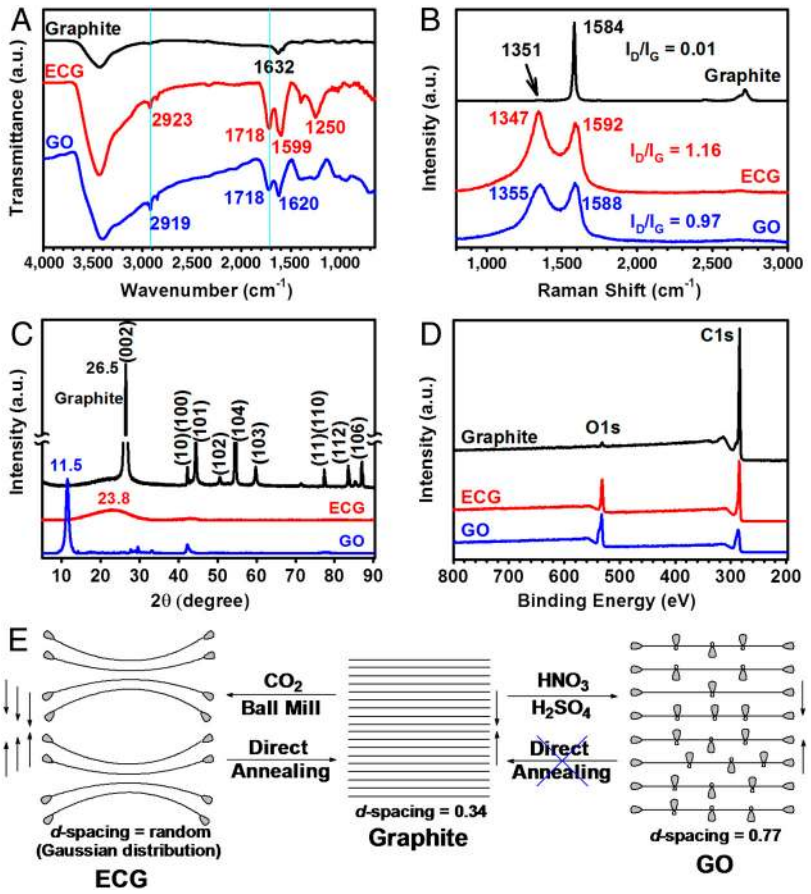

Fig. 3. (*A*) FTIR spectra (KBr pellets); (*B*) Raman spectra; (*C*) XRD diffraction patterns; (*D*) XPS survey spectra of the pristine graphite, ECG and GO; (*E*) schematic presentation of samples in solid state.

a sp^3C-H peak at 2,939 cm^{-1} associated with defects (Figs. S2 and S6), along with the sp^2 peak at 2,919 cm^{-1} (Fig. 3*A*). These spectroscopic results are consistent with the scenario for the reactions given in Figs. 1*D* and Fig. S6, which show that the reactive carbon species (radicals, anions and cations), generated by homolytic and heterolytic cleavages of the graphitic C–C bonds during ball milling in the presence of dry ice, reacted with carbon dioxide (CO_2), followed by protonation with moisture in air (Fig. S2). In a control experiment, the sparkling was not occurred when the capsule was opened in nitrogen/moisture (80/20, v/v) or dry air condition (see, Movies S1, S2, and S3), implying that the origin of sparkling is due to the reaction of residual activated carbon species in the presence of both oxygen and moisture together. Furthermore, we charged the ball mill capsule with pristine graphite and dry ice without balls and sealed for 48 h under the same conditions as for ECG (see, Experimental Section in *Supporting Information*). No change in the carbon content was observed, indicating the ball-milling-induced carboxylation did not occur in the control experiment.

Powder samples were further characterized by Raman spectroscopic and X-ray diffraction (XRD) measurements. As can be seen in Fig. 3*B*, the pristine graphite showed the G and 2D bands at 1,584 and 2,970 cm^{-1}, respectively. Due to the large grain size of graphite (see, Fig. 2*A*), its D band at 1,351 cm^{-1} associated with the edge distortion is negligibly weak with a ratio of the D-band to G-band intensity (I_D/I_G) to be approximately 0.01 (Fig. 3*B*). In contrast, ECG showed a broad strong D band over 1,347 cm^{-1} with $I_D/I_G = 1.16$ (even slightly higher than $I_D/I_G = 0.97$ for the often more distorted GO), indicating significant edge distortion due to grain size reduction (see, Fig. 2*B*). To confirm the edge-selective carboxylation, we have performed micro-Raman measurements at the edge and within the basal plane on a large piece of ECG deliberately selected at a relatively short ball-milling time (approximately 24 h). As expected, the Raman spectrum from the edge shows a much higher I_D/I_G ratio (approximately 1.32) than the corresponding value (approximately 0.33) for the basal plane (Fig. S9*A*). Interestingly, only ECG clearly displays that the sp^3 peak at 1,134 cm^{-1} at the edge-on scan (arrow, Fig. S9*A*), while the pristine graphite (Fig. S9*B*) and GO (Fig. S9*C*) do not show sp^3 peak around 1,130 cm^{-1}. These results prop up the proposed mechanism for the edge-selective carboxylation of graphite by ball-mill process (Figs. 1*D* and Fig. S2).

XRD diffraction patterns in Fig. 3*C* show a strong [002] peak at 26.5° for the pristine graphite, corresponding to a layer-to-layer d-spacing of 0.34 nm, with all other peaks attributable to the expected three-dimensional diffraction lines from hexagonal graphite (h-graphite) (26). The large shift of the [002] peak from 26.5° to 11.5° (corresponding to an interlayer distance change from 0.34 nm to 0.77 nm), along with the significant intensity decrease for all the peaks, seen in Fig. 3*C* for GO indicates a lattice expansion with partial exfoliation. However, only a very weak broad band over 15–30° was observed for ECG, suggesting a high degree of edge-expansion in solid state (Fig. 3*E*).

Further evidence for the edge-carboxylation comes from the XPS spectroscopic measurements. As expected, Fig. 3*D* shows only a pronounced C 1 s peak at 284.3 eV for the pristine graphite with a trace amount of O (approximately 532 eV) arising from the physically adsorbed oxygen (6, 27). Upon exfoliation either by acid-oxidation in solution or ball milling in the presence of dry ice, the O 1 s peak intensity relative to the C 1 s peak increased significantly as suggested by Figs. S2 and S6*A*. The

observed higher C/O ratio (C/O = 6.16) for ECG than that (C/O = 0.64) for GO clearly indicates that GO contains more oxygen-rich functionalities (Fig. S6*A* and Table S2) than the ECG with its edge only being functionalized with carboxylic acid (Fig. S2 and Table S2). Together with the curve fittings, high-resolution XPS C 1 s and O 1 s spectra (Fig. S10), once again, show that the O component in ECG comes dominantly from O = C-OH, whereas GO contains C-OH (hydroxyl), C-O-C (epoxy) and O = C-OH (carboxyl). These XPS data are in a good agreement with the FTIR results (Fig. 3*A*) as well as the structures shown in Figs. S2 and S6*A* for ECG and GO, respectively. Solid-state ^{13}C magic-angle spinning (MAS) NMR spectrum of ECG given in Fig. S11 also agrees well with the reactions shown in Fig. S2. While peaks at around 130 and 190 ppm are associated with the graphitic sp^2C and carbonyl C in carboxylic acid, respectively, the peak centered at 60 ppm is attributable to the sp^3C, at which carboxylic acid is attached (structure 5 in Fig. S2*A*). Overall, the ^{13}C MAS NMR spectrum is in good accordance with structure **5** as highlighted in Fig. S2. Hitherto, on the basis of EA, TGA, SEM, TEM, FTIR, Raman, XRD, XPS, and NMR characterization, the structural changes from graphite to ECG and GO could be pictorially summarized in Fig. 3*E*.

As envisioned from Fig. 3*E*, both the ball milling and GO process should lead to an increase in the surface area. It was found that Brunauer-Emmett-Teller (BET) surface area of pristine graphite, ECG and GO were 2.8, 389.4, and 29.8 m^2/g, respectively (Table S3). The profound increase (139 times) in the surface area of ECG by ball milling of the pristine graphite indicates the occurrence of a significant edge-lifting in ECG, as schematically shown in Fig. 3*E*. On the other hand, GO has approximately 10 times increase in surface area, in consistent with the slight interlayer expansion (Fig. 3*E*). Upon heat-treatment, the surface area of H-ECG is 631.8 m^2/g, which is approximately 6.9 times higher than that of H-GO (92.1 m^2/g) (Table S3). Thus, the H-ECG displays much higher double layer capacitance of 108 F/g (Fig. S12*A*) with good cycle stability (Fig. S12*B*), while H-GO has 72 F/g (Fig. S12*A*) with relatively poorer cycle stability (Fig. S12*B*).

The ability to carboxylate the edge of graphite flake simply by ball-milling with dry ice provides a great scope for dispersing the resultant ECG in various solvents and further modification with a large variety of functional moieties on demands via reactions characteristic of the carboxylic acid group (see, for example, Fig. S13). Indeed, ECG was found to be readily dispersible not only in protic solvents, such as basic water (containing ammonium hydroxide or potassium hydroxide), methanol, and isopropyl alcohol, but also polar aprotic solvents, including dimethyl sulfoxide (DMSO), *N*,*N*-dimethylformamide (DMF), *N*,*N*-dimethylacetamide (DMAc), and *N*-methyl-2-pyrrolidone (NMP) (Fig. S14*A*). Among all the solvents tested, NMP was found to be the best for dispersing ECG into a stable dispersion. The degree of dispersion roughly followed solvent polarity, which decreased with increasing number in Fig. S14*A*. ECG displayed the better dispersibility in the higher solvent polarity due to the presence of polar edge-carboxylic acids (-COOH). Both ECG and GO displayed a good stability of dispersion with similar Zeta-potential values of −34.2 and −35.1 mV, respectively, at the highest achievable concentration for GO in NMP (0.02 mg/mL, Fig. 4*A*). However, the concentration of ECG in NMP could be increased up to 0.06 mg/mL (three times that of GO in NMP) without precipitation and still with a Zeta-potential of −30.5 mV (Fig. 4*A*, *Inset*). It is well known that a Zeta-potential value either more negative or positive than ±30 mV is sufficient to ensure a good dispersion stability via charge repulsion (28). Therefore, the above results indicate that the strong repulsion force between the negatively charged -COO^- moieties, generated from the edge-carboxylic acids (-COOH) via ionization in the basic NMP medium (14), is responsible for the good dispersion of ECG in NMP.

To test the direct formation of molded objects for electronic applications, we first compressed (see, Experimental Section in *Supporting Information*) ECG and GO samples into pellets [diameter = 2.5 cm and thickness = ~200 μm, Figs. 4*B*(i) and 4*B*(ii), respectively], in solid state at room temperature (25 °C). ECG pellet shows electrical conductivity of 1.1×10^{-2} S/cm, which is 688 times higher than that of GO pellet (1.6×10^{-5} S/cm) (Table S4). Upon thermal annealing at 900 °C (decarboxylation) for 2 h under nitrogen, the ECG pellet remains intact as a cohesive film with electrical conductivity of 38 S/cm [Fig. 4*B*(iii)] whereas the compressed GO shattered into small pieces over the whole substrate surface [Fig. 4*B*(iv)] due to their different thermal behaviors (Note that gases evolve from edges and basal plane of GO) and hygroscopic natures (bound water)

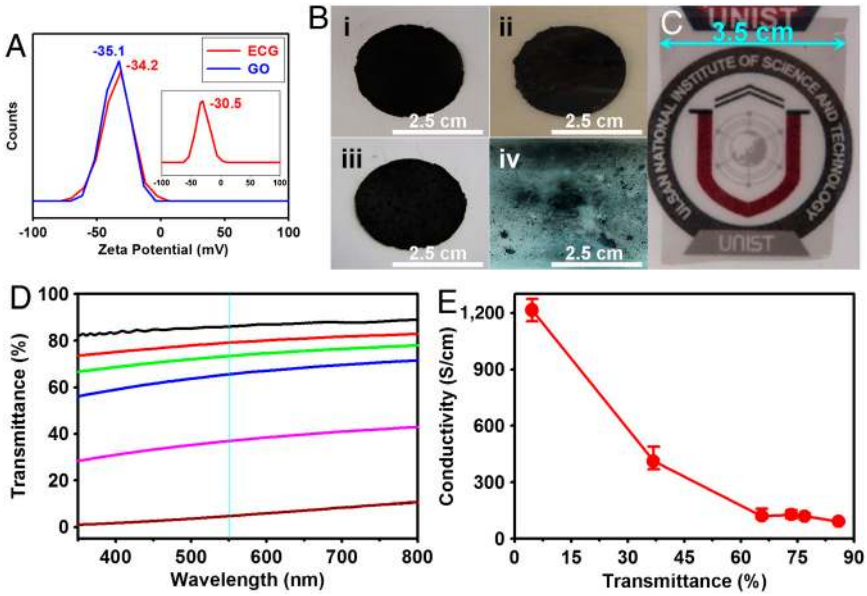

Fig. 4. (*A*) Zeta-potentials of ECG and GO at a concentration of 0.02 mg/mL in NMP. *Inset* is Zeta-potentials of ECG at a concentration of 0.06 mg/mL in NMP; (*B*) As-compressed pellets of (i) ECG and (ii) GO. After annealing at 900 °C for 2 h (iii) H-ECG and (iv) H-GO; (*C*) H-ECG thin film on PET (H-ECG/PET); (*D*) Optical transmittance of H-ECG/PET films. (*E*) Conductivity of the H-ECG/PET films vs. the calculated H-ECG transmittance at 550 nm.

indicated by Fig. S14*B*. Further plausible evidence for the difference between ECG (edge only functionalization) and GO (edge and basal plane functionalization), which has hygroscopic oxygenated groups on its edges and basal plane to cause an explosive expansion of GO pellets, comes from the TGA (Fig. S14*B*) and DSC (Fig. S14*C*) measurements. SEM image obtained from ECG after dispersed in NMP and reaggregated displays completely different surface morphology (Fig. S14*D*), indicating the presence of strong edge-hydrogen bonding. Therefore, ECG is more suitable than GO for the direct formation of conductive graphene pellet by high pressure compressing and subsequent thermal annealing. In the light of this observation, we also tested the possibility for the formation of large-area thin films by simple solution-casting. The stable dispersions of ECG in NMP with different concentrations were coated on SiO_2 (300 nm)/Si wafers (3.5 cm × 5.0 cm, the size of a graphene film to be formed is limited only by the size of the substrate used, and many substrates of different sizes can be used) and annealed at 900 °C to produce cohesive graphene films, which were able to be transferred on PET film (Fig. 4*C*). On the other hand, as observed in Fig. 4*B*(iv), direct annealing a GO thin film at 900 °C led to an explosion, leaving nothing on the SiO_2 (300 nm)/Si wafer.

In view of the above structural and mechanistic studies on reactions proposed in Fig. S2, we further treated ECG in the solid state at 900 °C under argon in order to restore the graphitic structure (**6–8** of Fig. S2) by thermal decarboxylation (CO_2-loosing) of ECG (**5** of Fig. S2). Indeed, the resultant heat-treated ECG (H-ECG) showed much narrowed D and G bands (Fig. S15*A*) with respect to the untreated ECG (see, Fig. 3*B*). H-ECG also displayed an additional peak at 1,090 cm^{-1} arising from those sp^3C-H edge bonds (29) highlighted in structures **7** and **8** of Fig. S2. Upon the heat treatment, the typical graphitic XRD diffraction pattern (see, Fig. 3*C*) reappeared for H-ECG (Fig. S15*B*), due probably to self-assembling induced by the strong π-π stacking between the newly regenerated graphitic basal planes (Fig. 3*E*). Therefore, ECG can be used as an ideal precursor for the formation of molded objects and/or large-area graphene films by low-cost, direct high pressure compressing as well as solution casting of its stable dispersion followed by thermal decarboxylation.

Depending on the film thickness, the optical transmittance at 550 nm of the solution-cast H-ECG films varied from 4.6% to 86.0% over a calculated thickness range of 2–14 nm (Fig. 4*D*) (7). Fig. 4*E* reproduces the percent transmittance-dependence of conductivity, which shows that the conductivity is inversely proportional to the optical transmittance (7). A simple conversion of the conductivity in the range of 90–1,200 S/cm into the corresponding sheet resistances from 53 to 0.58 kΩ/□ clearly shows that the conductivity of solution-cast H-ECG thin films are superb to their GO counterparts (approximately 100 kΩ/□) (11) by a few orders of magnitude even at the high transmittance region.

The methodology developed in this study could be regarded as a general approach toward low-cost, high-yield production of edge-selectively functionalized graphite (EFG) with various functional groups for multifunctional applications. To illustrate this point, we have also performed ball milling of the pristine graphite under the same condition as for ECG in the presence of ammonia (NH_3) or sulfur trioxide (SO_3), instead of dry ice (CO_2), to produce edge-amine (EAG) and edge-sulfonic-acid functionalized graphene (ESG). EA results showed that the atomic contents of nitrogen for EAG and sulfur for ESG are 4.49 and 9.35%, respectively (Table S5), in a good agreement with the TGA data (Fig. S16) as is the case for ECG. Apart from the above discussion, more other advantages for ECG with respect to GO can be found in Table S6.

In summary, we have developed a simple and eco-friendly (CO_2-capturing) ball-milling process to efficiently produce edge-carboxylated graphite (ECG) in solid state without involving hazardous chemicals. A reaction mechanism for the carboxylation by ball milling in the presence of dry ice and decarboxylation by thermal annealing ECG (H-ECG) under nitrogen was proposed and confirmed by various microscopic and spectroscopic measurements. The resultant ECG was demonstrated to be highly dispersible in various polar solvents suitable for solution casting. The ECG and H-ECG exhibited many superior structure-property characteristics with respect to its GO and H-GO counterparts. Thus, the ball-milling technique developed in this study could be regarded as a general approach toward low-cost, high-yield production of edge-functionalized graphene (EFG) with various functional groups of practical significance for mass production of multifunctional materials and devices based on graphene materials.

Materials and Methods

Graphite was obtained from Alfa Aesar (natural, 100 mesh, 99.9995% metals basis, Lot#14735) and used as received. Dry ice was purchased from Hanyu Chemical Inc., Korea. All other solvents were supplied by Aldrich Chemical Inc. and used without further purification, unless otherwise specified.

Edge-carboxylation of graphite (ECG) was prepared by ball milling of the pristine graphite in a planetary ball-mill machine in the presence of dry ice at 500 rpm. In a typical experiment, 5 g of the pristine graphite and 100 g of dry ice were placed into a stainless steel capsule containing stainless steel balls of 5 mm in diameter. The capsule was then sealed and fixed in the planetary ball-mill machine, and agitated with 500 rpm for 48 h. The resultant product was further Soxhlet extracted with 1 M aqueous HCl solution to completely acidify carboxylates and to remove metallic impurities, if any. Final product was freeze-dried at −120 °C under a reduced pressure (0.05 mmHg) for 48 h to yield 6.28 g (pristine graphite captured 1.28 g of CO_2 during mechanochemical cracking) of dark black powder. Detailed procedure is described in the *Supporting Information* (SI).

ACKNOWLEDGMENTS. This work was supported by World Class University (WCU), US-Korea NBIT and Basic Research Laboratory (BRL) programs through the National Research Foundation (NRF) of Korea and US Air Force Office of Scientific Research (AFOSR).

1. Geim AK, Novoselov KS (2007) The rise of graphene. *Nat Mater* 6:183–191.
2. Novoselov K, et al. (2004) Electric field effect in atomically thin carbon films. *Science* 306:666–669.
3. Berger C, et al. (2006) Electronic confinement and coherence in patterned epitaxial graphene. *Science* 312:1191–1196.
4. Kim KS, et al. (2009) Large-scale pattern growth of graphene films for stretchable transparent electrodes. *Nature* 457:706–710.
5. Li X, et al. (2009) Large-area synthesis of high-quality and uniform graphene films on copper foils. *Science* 324:1312–1314.
6. Stankovich S, et al. (2007) Synthesis of graphene-based nanosheets via chemical reduction of exfoliated graphite oxide. *Carbon* 45:1558–1565.
7. Bae S, et al. (2010) Roll-to-roll production of 30-inch graphene films for transparent electrodes. *Nat Nanotechnol* 5:574–578.
8. Li D, et al. (2008) Processable aqueous dispersions of graphene nanosheets. *Nat Nanotechnol* 3:101–105.
9. Niyogi S, et al. (2006) Solution properties of graphite and graphene. *J Am Chem Soc* 128:7720–7721.
10. Xu Y, et al. (2008) Flexible graphene films via the filtration of water-soluble noncovalent functionalized graphene sheets. *J Am Chem Soc* 130:5856–5857.
11. Eda G, Fanchini G, Chhowalla M (2008) Large-area ultrathin films of reduced graphene oxide as a transparent and flexible electronic material. *Nat Nanotechnol* 3:270–274.
12. Hummers WS, Offeman RE (1958) Preparation of graphitic oxide. *J Am Chem Soc* 80:1339–1339.
13. Park S, Ruoff RS (2009) Chemical methods for the production of graphenes. *Nat Nanotechnol* 4:217–224.
14. Becerril HA, et al. (2008) Evaluation of solution-processed reduced graphene oxide films as transparent conductors. *Acs Nano* 2:463–470.
15. Cai W, et al. (2008) Synthesis and solid-state NMR structural characterization of 13C-labeled graphite oxide. *Science* 321:1815–1817.
16. Fan X, et al. (2008) Deoxygenation of exfoliated graphite oxide under alkaline conditions: A green route to graphene preparation. *Adv Mater* 20:4490–4493.
17. Lerf A, He H, Forster M, Klinowski J (1998) Structure of graphite oxide revisited. *J Phys Chem B* 102:4477–4482.
18. Shin HJ, et al. (2009) Efficient reduction of graphite oxide by sodium borohydride and its effect on electrical conductance. *Adv Funct Mater* 19:1987–1992.
19. Wang X, Zhi L, Mullen K (2008) Transparent, conductive graphene electrodes for dye-sensitized solar cells. *Nano Lett* 8:323–327.

20. Boukhvalov DW, Katsnelson MI (2008) Modeling of graphite oxide. *J Am Chem Soc* 130:10697–10701.
21. Gibbins J, Chalmers H (2008) Carbon capture and storage. *Energy Policy* 36:4317–4322.
22. Hernandez Y, et al. (2008) High-yield production of graphene by liquid-phase exfoliation of graphite. *Nat Nanotechnol* 3:563–568.
23. Stankovich S, Piner RD, Nguyen SBT, Ruoff RS (2006) Synthesis and exfoliation of isocyanate-treated graphene oxide nanoplatelets. *Carbon* 44:3342–3347.
24. Eda G, Chhowalla M (2010) Chemically derived graphene oxide: Toeards large-area thin-film electronics and optoelectronics. *Adv Mater* 22:2392–2415.
25. Dreyer DR, et al. (2010) The chemistry of graphene oxide. *Chem Soc Rev* 39:228–240.
26. Li ZQ, et al. (2007) X-ray diffraction patterns of graphite and turbostratic carbon. *Carbon* 45:1686–1695.
27. Collins PG, Bradley K, Ishigami M, Zettl A (2000) Extreme oxygen sensitivity of electronic properties of carbon nanotubes. *Science* 287:1801–1804.
28. Everett DH (1988) *Basic Principles of Colloid Science* (Royal Society of Chemistry, London).
29. Fenske MR, et al. (1947) Raman spectra of hydrocarbons. *Anal Chem* 19:700–765.